JOURNAL OF GEOPHYSICAL RESEARCH, VOL. 104, NO. D24, PAGES 31,721–31,730, DECEMBER 27, 1999

Cirrus optical thickness and crystal size retrieval from ATSR-2 data using phase functions of imperfect hexagonal ice crystals

Wouter H. Knap, Michael Hess,[1] Piet Stammes, and Robert B. A. Koelemeijer
Royal Netherlands Meteorological Institute (KNMI), De Bilt

Phil D. Watts
Rutherford Appleton Laboratory, Chilton, Didcot, Oxon, United Kingdom

Abstract. Along Track Scanning Radiometer 2 (ATSR-2) measurements made over a tropical cirrus anvil are analyzed on the basis of radiative transfer calculations for clouds consisting of imperfect hexagonal ice crystals. Reflectivity measurements made at two wavelengths (0.87 μm, nonabsorbing; 1.6 μm, absorbing) and two viewing directions (nadir and forward) are considered. Model calculations for a cloud consisting of single-sized imperfect hexagonal ice crystals adequately explain the gross features of the ATSR-2 reflectivity measurements. Retrieved values of optical thickness and crystal size reveal no discernible relationship between these quantities. Nadir-derived and forward-derived optical thickness and crystal size are compared for both imperfect and near-perfect hexagonal crystals. For these two crystal shapes, there appears to be a moderate trade-off in consistent retrieval of crystal size versus retrieval of optical thickness. Consistent retrieval of crystal size is found for imperfect crystals. We find an average crystal size (defined as maximum crystal dimension) of 63 ± 4 μm for a model cloud consisting of imperfect hexagonal columns. For imperfect hexagonal plates a somewhat larger value is retrieved: 71 ± 3 μm. Both retrieved sizes suggest that the cloud system consisted of relatively small ice crystals.

1. Introduction

The importance of cirrus clouds in the radiation balance of the Earth's atmosphere and their great significance in the climate system has been mentioned frequently in recent literature [e.g., *Liou*, 1986; *Stephens et al.*, 1990]. Whether these clouds tend to cool or heat the earth depends on the radiative properties, which in turn depend on the microphysical composition of the clouds. Owing to the high altitude of cirrus cloud, the microphysical composition has only recently been studied through the availability of aircraft and satellites. The latter in particular provide an excellent opportunity for deriving microphysical parameters of cloud systems on the scales required by, e.g., general circulation models.

The retrieval of cloud parameters from satellite measurements requires detailed modeling of the radiative properties of clouds, solving both the problem of single and multiple scattering. As for ice clouds, the modeling of the single scattering properties is particularly difficult because of the complexity and diversity of the shape of the ice crystals. Owing to the fact that ice cloud particles are nonspherical and irregular, a rigorous theoretical description of the radiative properties (such as Mie theory for liquid water droplets) is virtually impossible. Fortunately, atmospheric ice crystals are often large enough to obtain a reasonable approximation by means of geometrical optics. In these cases, ray-tracing techniques can be used to obtain the single scattering properties of ice crystals [e.g., *Wendling et al.*, 1979; *Cai and Liou*, 1982; *Takano and Jayaweera*, 1985; *Macke*, 1994],

In this paper we analyze Along Track Scanning Radiometer 2 (ATSR-2) measurements made over an area of gradually thinning anvil cloud, streaming off the top of a deep-convective cloud system in the tropical North Pacific. Two ATSR-2 viewing directions (nadir and forward) and two wavelengths (the nonabsorbing 0.87 μm and the absorbing 1.6 μm) are considered. The analysis is performed on the basis of single scattering calculations for hexagonal ice crystals. The concept of ray tracing was used to calculate the single scattering properties of these crystals. Since the shape of natural ice crystals in cirrus clouds is likely to deviate from perfect hexagons, the natural shape was mimicked by means of introducing a random variation in photon paths at air/ice interfaces during the ray-tracing procedure [following *Macke et al.*, 1996; *Hess et al.*, 1998]. With respect to single scattering properties, the resulting imperfect or irregular ice crystals seem to bridge the gap between perfect hexagonal columns and complex-shaped models for natural ice crystals, such as disordered fractals.

The main goal of our investigation is to explore the possibilities of using phase functions of imperfect hexagonal ice crystals for simulating measured reflectivities over cirrus and, by considering the inverse problem, retrieving crystal

[1]Now at German Remote Sensing Data Center, DLR-Oberpfaffenhofen, Wessling, Germany.

Paper number 1999JD900267.
0148-0227/99/1999JD900267$09.00

size and optical thickness from ATSR-2 measurements. In this paper we first describe the models we used for simulating single scattering by imperfect hexagonal ice crystals and multiple scattering by the cloudy atmosphere. Next, the study area and the ATSR-2 data used for the analysis are described. Then, to aid the interpretation of model calculations, some sensitivity experiments concerning particle size and shape, and degree of crystal distortion are presented. Before considering the actual retrieval, it is shown that a reasonable simulation of the ATSR-2 reflectivities can be obtained on the basis of a cloud consisting of single-sized crystals. Pixel-by-pixel retrieval of crystal size and optical thickness together with a brief error discussion are presented before conclusions are drawn in the final section.

2. Model Description

2.1. Single Scattering by Imperfect Hexagonal Ice Crystals

To calculate the single scattering properties of imperfect hexagonal ice crystals, we used the ray-tracing method described by *Hess et al.* [1998]. The code used by these authors is an extended version of the code described by *Hess and Wiegner* [1994]. The extension consists of the calculation of the full 4×4 scattering matrix and the application of statistical variations in photon paths. These statistical variations have been added to mimic deviations from the ideal hexagonal shape of the ice crystals. From now on, we will refer to the resulting crystals as imperfect crystals. In the present context, this statistical variation is considered to be the most important aspect of the method. Therefore we will confine ourselves to describing (briefly) this part of the ray-tracing procedure.

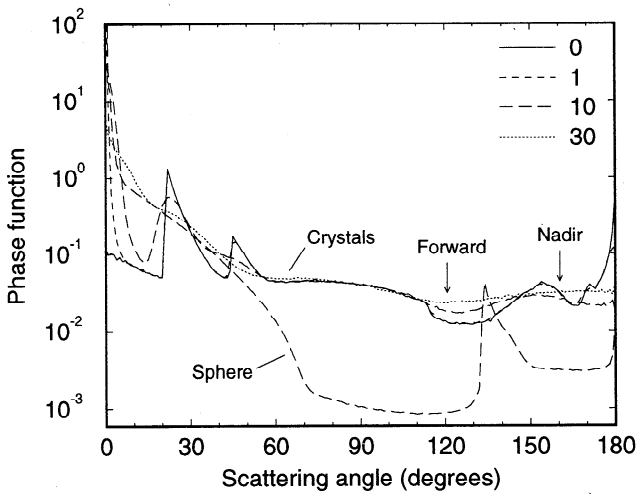

Figure 1. Phase function of imperfect hexagonal ice crystals for different values of the maximum tilt angle α (shown as numbers in the legend). The solid line ($\alpha = 0°$) corresponds to the undisturbed hexagonal column C2 (Table 1). The wavelength is 0.87 μm. Diffraction is excluded. For reasons of comparison (see section 4.2), the phase function of a sphere with radius 25 μm is also shown. The arrows indicate the scattering angles corresponding to two ATSR-2 viewing directions (see section 3). Note that the vertical axis has been cutoff at 10^2.

Possible deviations of the perfect hexagonal shape are mimicked by means of a random change in the normal vector of the crystal surface every time a photon interacts with an air/ice interface. The value of the tilt (zenith) angle is chosen randomly between 0 and a specified maximum value α. The tilt azimuth angle is distributed randomly between 0 and 2π. Refraction and reflection take place at the tilted surface element.

Figure 1 shows an example of the influence of the magnitude of α on the phase function. The calculations were performed for a nonabsorbing wavelength (0.87 μm; corresponding to one of the ATSR-2 bands) and diffraction was not included to avoid effects of particle size. The particles are oriented randomly in space. As many as 1,000,000 photon paths have been calculated. Figure 1 demonstrates that the significant features of the phase function (sharp peaks in the forward and backward direction, and the halos at 22° and 46°) become less prominent as the maximum tilt angle increases. For $\alpha = 30°$ the halos and other sharp features have disappeared and the phase function varies gently with the scattering angle. *Hess et al.* [1998] propose $\alpha = 30°$ as a suitable value for simulating the single scattering properties of irregular hexagonal crystals. Unless stated otherwise, this value has been used for the calculations presented in this paper.

2.2. Multiple Scattering

The calculations for multiple scattering of sunlight in a cloudy atmosphere were performed with the Doubling-Adding KNMI (DAK) model. As suggested by the name of this model, the problem of multiple scattering is solved by means of the doubling-adding method [*De Haan et al.*, 1987]. The model consists of a plane-parallel multilayered atmosphere over a Lambertian surface. A detailed description of DAK is given by *Stammes* [1994]. The present analysis is made on the basis of one of the output results of DAK: the reflectivity at the top of the Earth's atmosphere (TOA), defined by

$$R(\theta,\theta_o,\phi-\phi_o)=\frac{I(\theta,\theta_o,\phi-\phi_o)}{F_o\cos\theta_o}, \quad (1)$$

where I is the TOA atmospheric radiance, θ_o is the solar zenith angle, and πF_o is the incident solar irradiance perpendicular to the solar beam. The viewing geometry is defined by the viewing zenith angle θ and the relative viewing azimuth angle $\phi - \phi_o$.

The tropical model atmosphere for temperature, pressure and ozone was taken from *Anderson et al.* [1986]. Because of the high altitude of cirrus clouds, the effect of aerosols on the reflectivity is expected to be small, so the model atmosphere contained no aerosols. For the same reason, and because near-infrared wavelengths are considered, the Rayleigh optical thickness of the air layer above the cloud is small. This implies that the effect of polarization on the reflectivity, due to Rayleigh scattering, can safely be neglected. For near-infrared wavelengths and for the cloud particle sizes considered, the degree of polarization for cloud particle scattering is small, and was also neglected. The surface albedo was fixed to a wavelength-independent value of 0.05 (estimated value of the albedo of a sea surface). To simulate a cirrus cloud, ice crystals were mixed into a certain atmospheric layer. Phase functions of the ice crystals were

calculated for various particle sizes and shapes using the ray-tracing model described in the previous section. To produce the input needed for DAK, the phase functions were expanded in generalised spherical functions [*De Rooij and Van der Stap,* 1984].

2.3. Treatment of the Forward Peak in the Phase Function

In practice, the number of expansion coefficients needed to obtain a good representation of the forward peak in the phase function was too large to handle (several thousands for the larger particles). To solve this problem, the forward peak was cut off at scattering angle $\Theta = \Theta_c$, i.e., for scattering angles between 0 and Θ_c the phase function was fixed to its value at $\Theta = \Theta_c$ (following the delta approximation of *Potter* [1970]). The number of photons scattered in the forward direction in largely reduced by truncating the phase function. The photons that were originally scattered in the forward direction are treated as if they are not scattered at all.

For the crystals considered here, $\Theta_c = 1°$ was large enough and a good fit of the adjusted phase function could be obtained with 750 expansion coefficients. Since the delta approximation implies that less photons are scattered into the forward direction, the scattering and extinction coefficients are reduced. To compensate for the increase in unscattered energy, the optical thickness was adjusted in the DAK model according to

$$\tau_a = (1-\delta\omega_o)\tau. \tag{2a}$$

Here τ_a and τ are the adjusted and real optical thickness, respectively, ω_o is the single-scattering albedo corresponding to the original phase function, and δ is the amount of energy that is removed by cutting off the phase function $p(\Theta)$ at scattering angle $\Theta = \Theta_c$:

$$\delta = \int_0^{\Theta_c} \{p(\Theta) - p(\Theta_c)\}\, d\Omega. \tag{2b}$$

All calculations presented in this paper have been performed using cutoff phase functions at $\Theta_c = 1°$ and adjusted optical thicknesses τ_a. However, the results for the retrieved optical thickness are presented in terms of τ.

3. ATSR-2 Data

The ATSR-2 (an imaging radiometer on board the ESA/ ERS-2 satellite) produces images of the Earth at three visible/near-infrared wavelengths (0.55, 0.67, and 0.87 μm) and four infrared wavelengths (1.6, 3.7, 11, and 12 μm). The instrument has been designed to observe the same scene in "nadir" view (zenith angle between 0° and 25°) and in "forward" view (zenith angle between 52° and 55°). The spatial resolution at nadir is about 1 × 1 km^2. Owing to the spectral and dual-view design of ATSR-2, the instrument has a wide variety of applications, one of which is to detect sea surface temperatures. *Watts* [1995] and *Baran et al.* [1998] have pointed out the possibilities for retrieval of cloud microphysical parameters.

The image used for analysis has been acquired over the Pacific Ocean (14°N, 134°E) on September 6, 1996 (Figure 2a). It contains large convective clouds (typical horizontal scale: 50-100 km), grouped in a large overall structure (300-500 km and off the image). An area containing gradually thickening anvil cloud was selected for analysis puposes. The solar zenith angle at the time of the overpass is $\theta_o = 23°$. The cloud was viewed under the following angles: $\theta = 3°$, $\phi - \phi_o = 157°$ (nadir), and $\theta = 54°$, $\phi - \phi_o = 86°$ (forward). The nadir and forward viewing directions correspond to scattering angles of 161° and 121°, respectively (see also Figure 1).

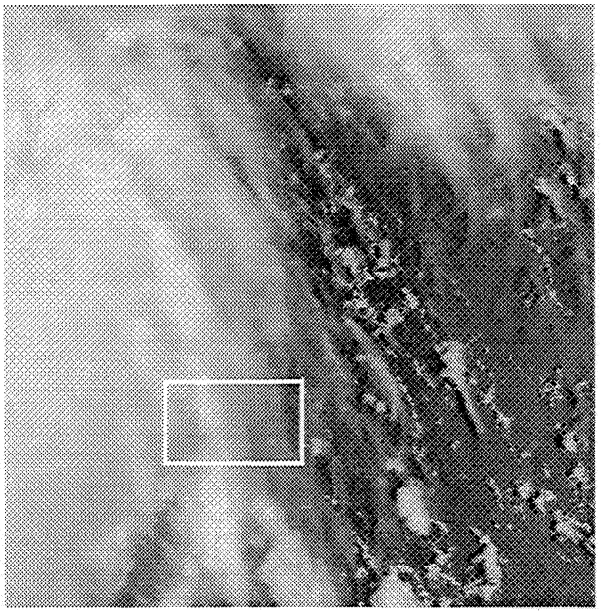

Figure 2a. ATSR-2 nadir scene of tropical convective clouds, acquired over the Pacific Ocean (14°N, 134°E) on September 6, 1996. The selection indicated contains a gradually thickening anvil cloud, selected for analysis purposes in the present paper.

To correct for the effects of parallax and cloud drift (clouds may drift up to several kilometers in the two minutes that elapse between nadir and forward measurements), the two images had to be colocated at cloud top height. This was done by shifting the images by eye until no apparent movement of the cloud resulted when the images were animated.

Figure 2b shows the ATSR-2 measurements corresponding to the selection indicated in Figure 2a. Plotted is the TOA reflectivity at 1.6 μm versus the reflectivity at 0.87 μm for both viewing directions. Figure 2b reveals two main features: (1) for small reflectivity the relationship between the reflectivities at the two wavelengths considered is approximately linear (see left branch of the reflectivity curves), whereas for increasing reflectivity the gradient $dR(\lambda$=1.6 μm$)/dR(\lambda$=0.87 μm) decreases and eventually vanishes (see right branch of the reflectivity curves); (2) at the right ends of the reflectivity curves, R(forward) is larger than R(nadir) at 1.6 μm, whereas R(forward) is smaller than R(nadir) at 0.87 μm. The rapidly decreasing gradient for increasing reflectivity (i.e., for increasing optical thickness) is caused by the fact that the imaginary part of the refractive index at 1.6 μm is 3 orders of magnitude larger than at 0.87 μm [*Warren*, 1984]. The associated contrast in absorption becomes increasingly important as the number of scattering events increases, i.e., as the cloud becomes optically thicker and the reflectivity increases. As for feature 2, model

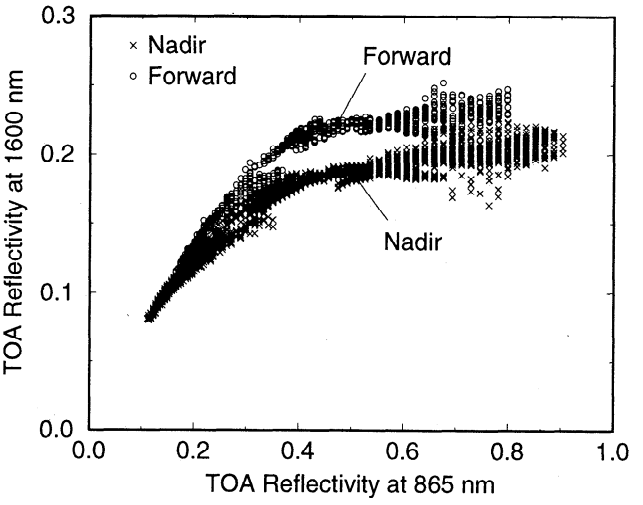

Figure 2b. Nadir and forward ATSR-2 reflectivity measurements at 0.87 and 1.6 μm, corresponding to the selection indicated in Figure 2a. The precise viewing geometry is described in the text.

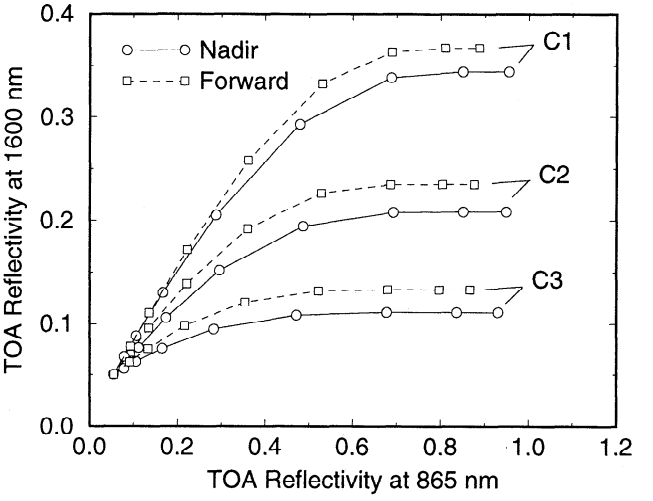

Figure 3. Computed TOA reflectivity at 1.6 μm (absorbing) versus the same quantity at 0.87 μm (nonabsorbing) for clouds consisting of hexagonal columns C1, C2, or C3 (Table 1). The maximum tilt angle $\alpha = 30°$. Results for both the nadir and forward ATSR-2 viewing direction are shown. Following the curves from left to right the optical thickness increases according to the series 0, 0.5, 1, 2, 4, ..., 64.

calculations (not presented here) show that this feature occurs even for isotropic single scattering, which suggests that it can be explained in terms of multiple scattering.

4. Sensitivity Analysis

In this section it is investigated to what extent the simulated TOA reflectivity is sensitive to changes in crystal size and particle shape. Furthermore, the effect of the magnitude of the maximum tilt angle α (see section 2.1) is studied. All computations were performed for a stratiform cirrus cloud consisting of ice particles mixed into an atmospheric layer between 7 and 8 km altitude. The cloud optical thickness was varied according to the series: 0, 0.5, 1, 2, 4,.., 64 (9 values). The analysis is entirely focused on the 0.87 μm and 1.6 μm ATSR-2 reflectivity measurements presented in Figure 2b. Therefore the model calculations were performed for the solar and viewing geometry corresponding to this ATSR-2 scene.

Table 1 lists the dimensions of the hexagonal crystals used for the sensitivity analysis (sizes and names taken from COP data library of optical properties of hexagonal ice crystals [*Hess and Wiegner*, 1994]). Shown are the half-length of the a axis (a), the c axis (c), the aspect ratio ($c/2a$), and the maximum crystal dimension (D). For hexagonal columns $D = c$, whereas for plates $D = 2a$.

Table 1. Dimensions and Aspect Ratios of Hexagonal Crystals Used in the Present Study.

	Column			Plate
	C1	C2	C3	P2
a	10	22	41	30
c	30	60	130	12
D	30	60	130	60
$C/2a$	1.5	1.4	1.6	0.2

The symbols a and c indicate the half length of the a axis and the c axis, respectively. D is the maximum crystal dimension. All sizes are in micrometers.

4.1. Influence of Ice Crystal Size

Figure 3 shows the reflectivity at 1.6 μm versus the reflectivity at 0.87 μm for clouds consisting of the hexagonal columns C1, C2, or C3 (Table 1). Calculations for both viewing directions are shown. Anticipating on a comparison between these model calculations and the ATSR-2 measurements (section 5), we can already conclude that the gross features of the measurements seen in Figure 2b are well represented by the model. Figure 3 demonstrates that the reflectivity is sensitive to changes in the crystal size. The sensitivity is to a large extent determined by changes in ice absorption at the 1.6 μm wavelength; a larger (smaller) particle increases (decreases) the chance of a photon being absorbed.

4.2. Influence of Particle Shape

Figure 4 shows computed reflectivities for clouds consisting of four different particle shapes. The hexagonal column C2 serves as reference case (cf. Figure 3). The other particles are: the hexagonal plate P2 (see Table 1), an ice sphere with a radius of 25 μm (which is more or less an area-equivalent sphere for C2 and P2), and a hypothetical particle with an isotropic phase function (single scattering albedo equal to that of C2). We present results for the nadir viewing direction only, because the forward viewing direction gives similar results. The figure shows that the hexagonal plate P2 gives results comparable to the hexagonal column C2. Note that even though the curves are quite similar, individual differences for *fixed* optical thickness can be substantial (particularly for the non-absorbing wavelength). The sphere and the "particle" with an isotropic phase function clearly represent two extreme cases. The reflectivity of the cloud consisting of spherical ice particles is strongly suppressed at $\lambda = 1.6$ μm. Closer agreement with the reflectivity curves of the hexagonal particles can be obtained by increasing the single scattering albedo through decreasing the volume of the sphere

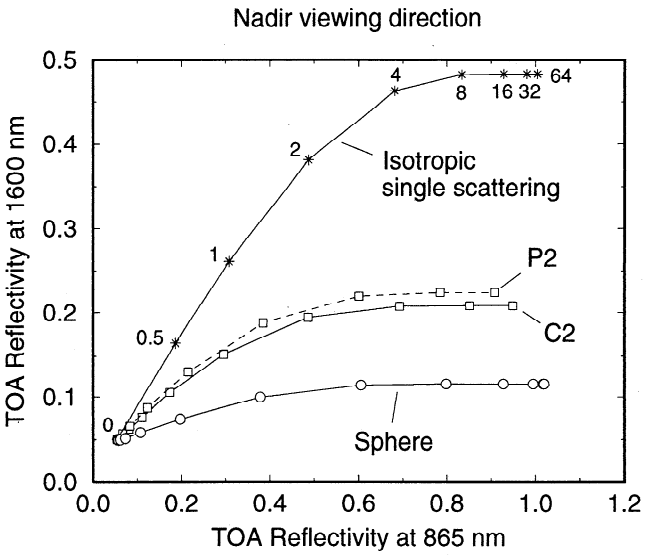

Figure 4. Effect of particle shape on the relationship between the reflectivity at 1.6 μm and the reflectivity at 0.87 μm. Four different particles are indicated: a hexagonal column (C2), a hexagonal plate (P2), a sphere (radius: 25 μm) and a hypothetical particle with an isotropic phase function. The labels indicate optical thickness.

(not shown). The reduction in the reflectivity at λ = 1.6 μm can be explained on the basis of the single scattering properties of the hexagonal particle and the sphere. The phase function of these particles (Figure 1) shows that scattering in the nadir viewing direction is much less probable for the sphere than for the hexagonal particle. This applies to the phase functions at λ = 0.87 μm as well as at λ = 1.6 μm (the latter are not shown). At the nonabsorbing wavelength (0.87 μm), and for high optical thickness, using phase functions of crystals and spheres result in almost equal reflectivities. In that case, multiple scattering obscures single scattering features. For a cloud consisting of isotropically reflecting particles, the chance of a photon to be scattered in the viewing direction is for both wavelengths roughly two orders of magnitude larger than for the hexagonal particle. This results in the significant increase in the reflectivity for both the absorbing and non-absorbing wavelength, as can be seen in Figure 4.

4.3. Influence of Maximum Tilt Angle

Figures 5a and 5b show how the computed reflectivities of clouds consisting of imperfect hexagonal ice crystals are influenced by the magnitude of the maximum tilt angle α (see section 2.1). The computations were performed for the hexagonal column C2 and for α = 1° and α = 30°. For both viewing directions, a reduction in α mainly results in a lowering of the curve. The effect is more pronounced in the forward viewing direction than in the nadir viewing direction. This can be explained by considering the phase function for the different tilt angles (Figure 1). At a scattering angle of 121°, a decrease in the maximum tilt angle leads to a significant reduction in the magnitude of the phase function, which in turn suppresses the chance of a photon to be scattered in the forward viewing direction. In the nadir viewing direction (scattering angle: 161°), the sensitivity of the magnitude of the phase function for changes in α is relatively small, which explains the limited effect shown Figure 5a.

5. Comparison of Model Calculations and ATSR-2 Measurements

In this section we will bring together model calculations and ATSR-2 measurements of the observed cirrus cloud system. Single scattering properties were calculated on the basis of randomly oriented imperfect hexagonal columnar ice crystals of type C2 (Table 1). The stratiform cirrus model cloud extends between 7 and 8 km and has a variable optical thickness (τ = 0.5, 1, 2, 4, 8, 16, 32, 64).

Figures 6a and 6b show plots of $R(\lambda$=1.6 μm) against $R(\lambda$=0.87 μm) containing the model calculations and ATSR-2 measurements for both ATSR-2 viewing directions. The main features of the measurements, i.e more or less linear behaviour for small optical thickness (say $\tau \leq 2$) and

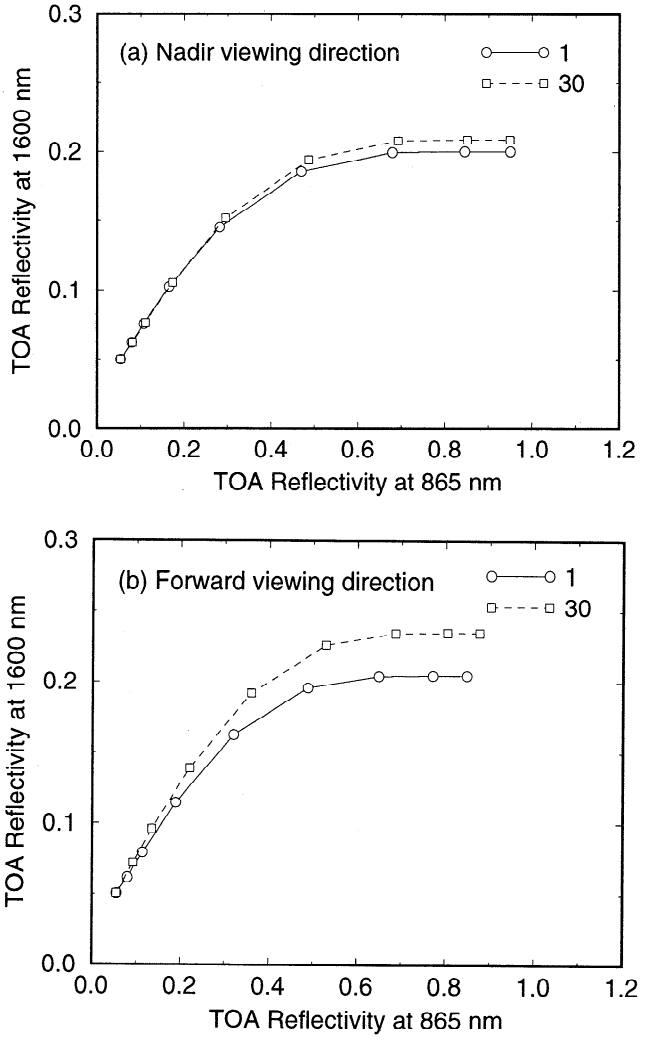

Figure 5. Effect of the maximum tilt angle α on the relationship between the 1.6 μm and 0.87 μm (a) nadir and (b) forward reflectivity of a cirrus cloud. Results are shown for α = 1° and α = 30°. Following the curves from left to right the optical thickness increases according to the series 0, 0.5, 1, 2, 4, .., 64.

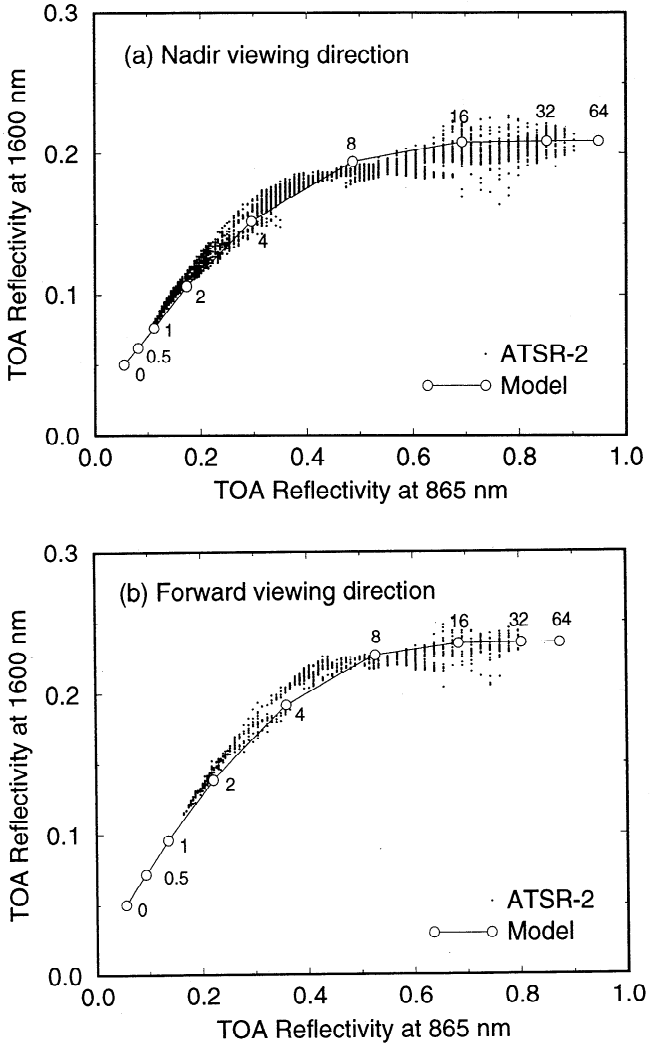

Figure 6. Model calculations for the (a) nadir and (b) forward viewing direction for a cloud consisting of hexagonal columns of type C2 with $\alpha = 30°$, together with the ATSR-2 measurements. The numbers next to the data points indicate model optical thicknesses.

flattening of the curve for higher optical thickness, are very well reproduced by the model. The model calculations are often within or only just outside the scatter of the measurements, which suggests that the "average" particle occurring in the observed cirrus cloud system can be represented fairly well by the column C2. By comparing Figures 6 and 3 it can be concluded that the scatter in the measurements suggests a modest variability in crystal size which is well within the range C1 - C3 (Table 1). The next section will deal with the retrieval of crystal size and optical thickness for each pixel of the ATSR-2 scene considered.

6. Retrieval of Optical Thickness and Crystal Size

6.1. Method and Error Analysis

To retrieve optical thickness (τ) and crystal size (D) for all all pixels of the considered ATSR-2 scene, we constructed a database of reflectivities for various values of τ and D. Since the model assumes a plane-parallel homogeneous cloud consisting of single-sized ice crystals, the retrieval process results in a single pair of τ and D for each ATSR-2 pixel. Therefore retrievals of τ and D should be regarded as effective values of optical thickness and crystal size, representative of an entire ATSR-2 pixel. To characterize the crystal size we took for D the maximum crystal dimension. The optical thickness was varied according to the series $2^{n/2}$ where $n = -1, 0, .., 11$. D was increased linearly from 30 to 80 μm in steps of 5 μm. The aspect ratio of the hexagonal columns was fixed to 1.4 (corresponding to C2, see Table 1), which is in broad agreement with the fact that small hexagonal ice crystals, i.e. at close range of C2, show relatively little variation in shape [see *Auer and Veal,* 1970]. All calculations were performed for $\alpha = 30°$ and $\Theta_c = 1°$.

Figure 7 shows the calculations of the 0.87 and 1.6 μm nadir reflectivity as a function of optical thickness and crystal size. The domain of τ and D spans the range of the ATSR-2 measurements considered in the present paper (Figure 2b). Figure 7 shows that for optically thick clouds (say $\tau > 20$) the nonabsorbing and absorbing reflectivities are nearly orthogonal. *Nakajima and King* [1990] obtained an analogous result for water clouds. For optically thin clouds both the 0.87 and 1.6 μm reflectivity depend on τ, which suggests that retrieval of the crystal size is less certain for this type of clouds (further discussion is given below).

In order to retrieve τ and D for an arbitrary pair of ATSR-2 measurements, the model calculations of $R(\lambda$=0.87 μm) and $R(\lambda$=1.6 μm) were resampled to a high-resolution regular grid on the basis of quintic polynomial interpolation. The interpolation gives a near-perfect representation of the model calculations (differences in reflectivity << 0.01). The interpolated model reflectivity values were put into a table and by means of an iterative procedure a solution for τ and D was reached. The difference between measured ATSR-2 reflectivities and the reflectivities at the solution was always negligible.

For a proper interpretation of retrieved crystal size and optical thickness, we need to establish the sensitivity of D and τ for uncertainty in the ATSR-2 measurements. To do so, a random error of 0.01 (absolute) in $R(\lambda$=0.87 μm) and $R(\lambda$=1.6 μm) was assumed. For three typical values of optical thickness (high, $\tau \sim 30$; medium, $\tau \sim 10$; and low, $\tau \sim 2$) the corresponding errors in the retrieved D and τ were calculated (shown in Figure 7 as error bars). The error in τ is generally small; values of ± 2, ± 0.2, and ± 0.2 were calculated for high, medium and low τ, respectively. For high to medium τ the error in D increases slowly from ± 3 to ± 4 μm. However, for $\tau < 10$ the error in the retrieved crystal size increases rapidly; for $\tau \sim 2$ we find an error of ± 19 μm. In conclusion we may state that for optically thin clouds retrieved crystal sizes are highly uncertain.

6.2. Results

Figures 8a and 8b show plots of retrieved crystal size versus optical thickness, for nadir and forward viewing direction for the selection of the ATSR-2 scene shown in Figure 2. At first sight, D and τ seems to be positively correlated for $\tau < 10$. However, in view of the previous discussion, the uncertainty in D for optically thin clouds is too large to support any statistical correlation between D and τ. The absence of an apparent relationship between crystal size

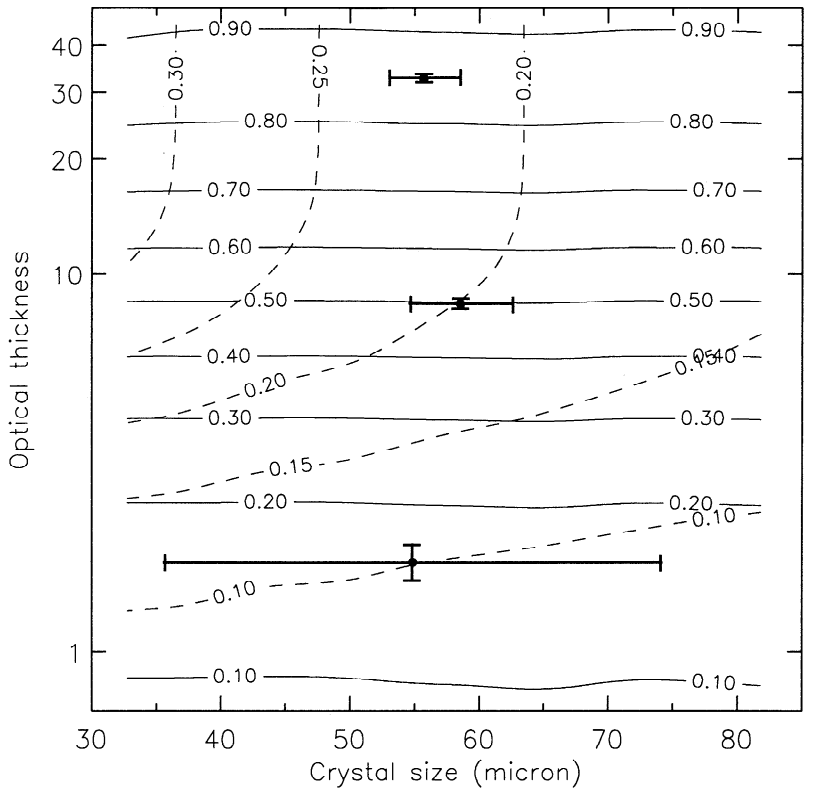

Figure 7. Modeled reflectivity as a function of optical thickness and crystal size (largest crystal dimension) for $\lambda = 0.87$ μm (solid curves) and $\lambda = 1.6$ μm (dashed curves). The error bars indicate uncertainty in retrieved optical thickness and crystal size resulting from an absolute random error of 0.01 in the ATSR-2 reflectivities (see section 6.2).

and optical thickness, $\delta D/\delta\tau \sim 0$, is in agreement with results presented by *Watts and Baran* [1997] and *Watts et al.* [1998]. In order to avoid large retrieval errors, from now we will only consider those values of D for which $\tau > 10$.

On average we find $D = 64 \pm 4$ μm (nadir) and $D = 62 \pm 3$ μm (forward), so there is no discernible difference between nadir-derived and forward-derived crystal size. The same conclusion can be drawn from Figure 9a, in which nadir- and forward-derived crystal size are plotted against each other. Without distinguishing between nadir and forward viewing direction the average crystal size appears to be 63 ± 4 μm. Comparing this with the results compiled by *Dowling and Radke* [1990], who give a typical crystal size of cirrus clouds of 250 μm (range: 1 - 8000 μm), we may conclude that the

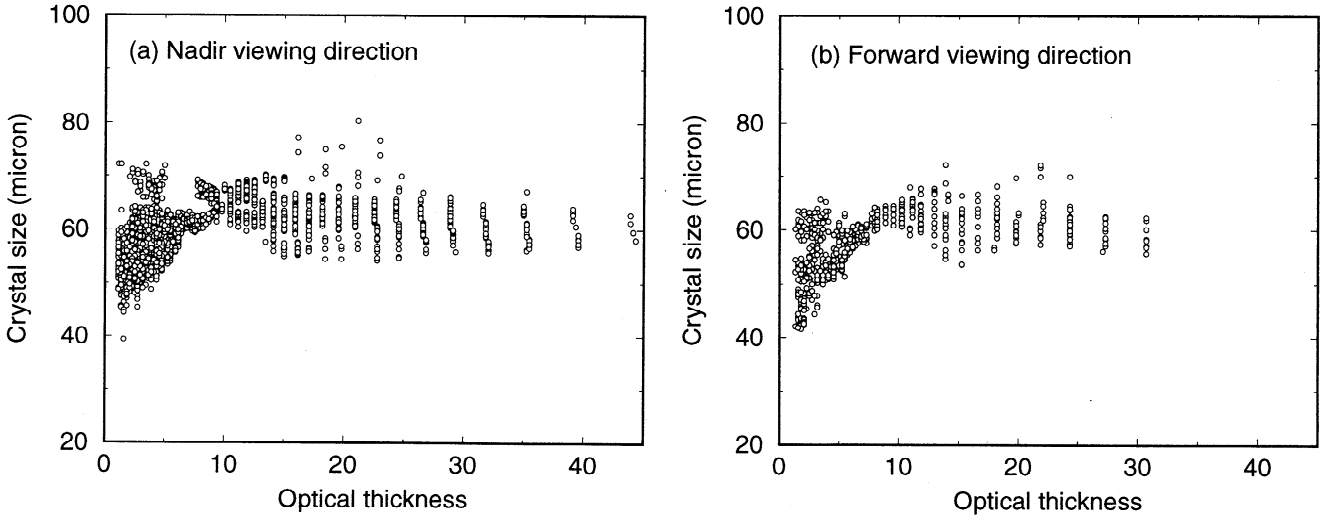

Figure 8. Crystal size (largest crystal dimension) as a function of optical thickness, as derived from (a) nadir and (b) forward ATSR-2 measurements.

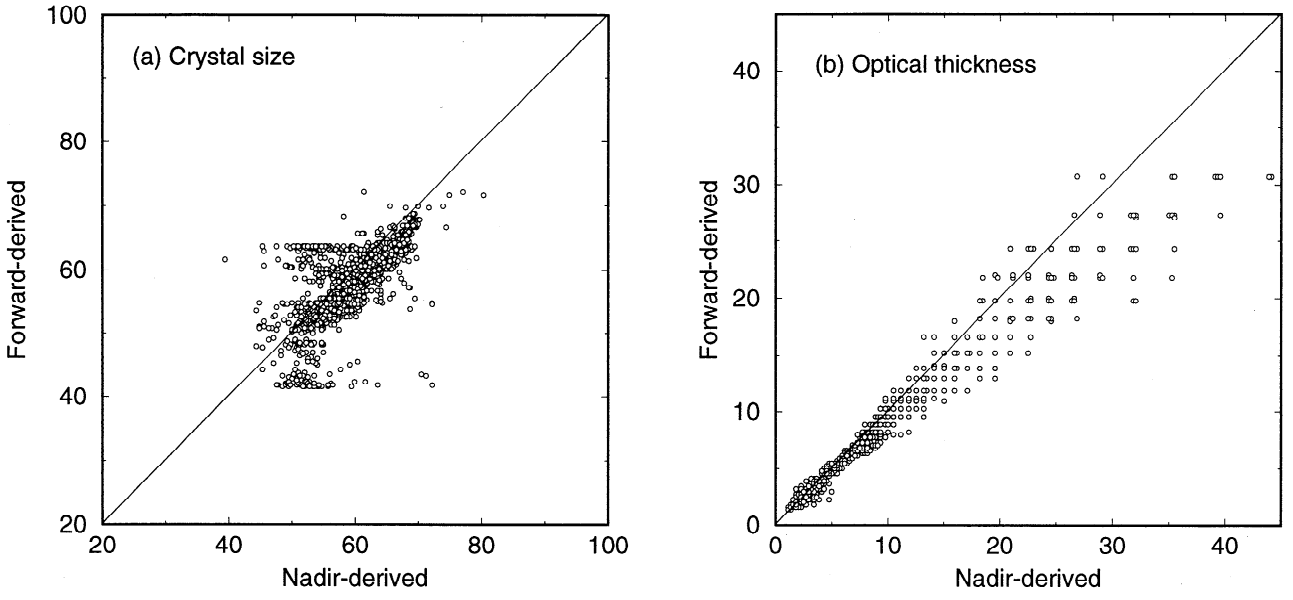

Figure 9. Forward-derived versus nadir-derived (a) crystal size (maximum crystal dimension, in μm) and (b) optical thickness.

ATSR-2 retrieved crystal sizes are relatively small. Our results are in broad agreement with ATSR-2 retrieved crystal sizes presented by *Watts et al.* [1998]. These authors considered five areas in the tropics and derived, on the basis of polycrystal phase functions, crystal sizes of 50, 83, 87, 94, and 73 μm. Again, our case suggests relatively small crystals.

As for optical thickness, Figure 9b reveals a trend for nadir-derived τ and forward-derived τ to diverge as τ increases. Further discussion on this point is given in section 6.3.

6.3. Discussion

In line with the sensitivity analysis presented in section 4, in the present section the retrieval of D and τ is reconsidered in view of changes in the degree of crystal imperfectness and in crystal shape. First, a comparison is made between retrievals for $\alpha = 1°$ (near-perfect hexagon) and $\alpha = 30°$ (imperfect hexagon); next the effect of using hexagonal plates instead of columns is discussed.

We can expect the retrieved crystal size to decrease as the crystal shape approaches an ideal hexagon (i.e., if α decreases) (see Figures 3 and 5). For reasons explained in section 4.3, the effect of reducing α on the 1.6 μm reflectivity is most pronounced for the forward viewing direction, so the crystal size reduction should be more obvious for forward-viewing than for nadir-viewing. This presupposition is confirmed by Table 2, which shows mean retrieved values of D for $\alpha = 1°$ and $\alpha = 30°$. Going from $\alpha = 30°$ to $\alpha = 1°$, D decreases by 3 μm for nadir viewing and 10 μm for forward viewing. In view of a retrieval uncertainty of 3 - 4 μm (see section 6.1), the latter reduction can be regarded as significant. Apparently, nadir-derived and forward-derived crystal size become less consistent as the crystal shape becomes more ideal. According to results of linear regression (see Table 2), the opposite is true for optical thickness: nadir-derived and forward-derived τ agree better for $\alpha = 1°$ than for $\alpha = 30°$. To find out if there is a general trade-off in consistent retrieval of D versus retrieval of τ, retrievals for values of α between 1° and 30° need to be considered. This has not been pursued in the present work.

Crystal sizes were also retrieved for a cloud consisting of imperfect ($\alpha = 30°$) hexagonal plates, instead of columns. The aspect ratio was fixed to 0.2, corresponding to the plate P2 (Table 1). The results of this experiment are summarised in Table 2. We find that on average $D = 69 \pm 3$ μm for nadir viewing and $D = 72 \pm 3$ μm for forward viewing, so the retrieved average crystal size for imperfect plates is 5 to 10 μm larger than for columns. Differences between nadir and

Table 2. Summary of the Effect of a Change in the Maximum Tilt Angle α (Section 2.1) and Crystal Shape (i.e., Column or Plate) on Nadir-Derived and Forward-Derived Crystal Size (Only for $\tau > 10$) and Optical Thickness (all τ).

			Average Crystal Size D, in μm ($\tau > 10$)		Linear Regression on τ (all τ)	
α	Shape	$C/2a$	Nadir-Derived	Forward-Derived	Slope	Intercept
1°	Column	1.4 (C2)	61 ± 3	52 ± 2	0.98	0.68
30°	Column	1.4 (C2)	64 ± 4	62 ± 3	0.81	0.91
30°	Plate	0.2 (P2)	69 ± 3	72 ± 3	0.80	0.86

The values $\alpha = 1°$ and $\alpha = 30°$ correspond to a near-perfect and an imperfect hexagonal crystal, respectively. The slope and intercept in the last two columns refer to linear regression on [τ(nadir), τ(forward)].

forward retrievals of D and τ prove to be similar for plates and columns.

7. Summary and Concluding Remarks

The analysis presented in this paper shows that the model, which is based on phase functions of imperfect hexagonal ice crystals for single scattering and the doubling-adding method for multiple scattering, is able to reproduce well the ATSR-2 cirrus reflectivity measurements. Model calculations of the reflectivity at 0.87 and 1.6 μm for a cloud consisting of single-sized imperfect hexagonal ice crystals (maximum dimension D = 60 μm) are generally within the scatter of the ATSR-2 measurements. This applies to both the nadir and forward viewing direction of ATSR-2.

If the model particle shape would resemble the real shape of the crystals in the cloud, one would expect retrievals for the forward and nadir viewing direction to be consistent. Even though the reverse is not necessarily true, it makes sense to compare both retrievals as a test for the assumed particle shape. For single scattering described by phase functions of imperfect hexagonal crystals, nadir-derived and forward-derived crystal sizes of the observed cloud system prove to be consistent. With regard to optical thickness τ, there is a trend for nadir-derived τ and forward-derived τ to diverge as τ increases. This trend is absent if single scattering is described by phase functions of near-perfect hexagons. On the other hand, nadir-derived and forward-derived crystal sizes show less agreement for near-perfect hexagons than for imperfect hexagons. To find out if there is a general trade-off in consistent retrieval of D versus τ, or if consistent retrievals can be obtained for some intermediate crystal shape, it is necessary to carry out additional calculations for different degrees of crystal imperfectness. The ray-tracing code used allows one to generate phase functions for a number of hexagonal crystal shapes, ranging continuously from the perfect to the imperfect hexagon.

Besides using the imperfect hexagonal shape for describing the single scattering properties of the cloud particles, it would be interesting to extend our analysis by considering phase functions of polycrystals [*Macke et al.,* 1996]. Such an extension may focus on the nadir/forward (in)consistency of retrieved D and τ for the different crystal geometries, in order to shed light on possible differences in performance between imperfect hexagons and polycrystals. Since ATSR-2 employs only two viewing directions, unique identification of cloud particle shape is problematic. An instrument like POLDER (POLarization and Directionality of the Earth's Reflectances), with its multiview and polarization-detection capability, may have the potential to give the information needed to reveal the shape of cirrus ice crystals [*Chepfer et al.*, 1998]. Because the *Hess et al.* [1998] model produces the full 4×4 scattering matrix, and because our doubling/adding model can also deal with polarization, these models are suitable for the analysis of polarization measurements.

Despite some uncertainty in particle shape, the retrieved crystal sizes can be considered as realistic and not inconsistent with results presented by others. For $\tau > 10$, the average value we derived on the basis of phase functions of imperfect hexagonal columnar ice crystals is 63 ± 4 μm. For hexagonal plates, a somewhat larger value is derived: 71 ± 3 μm. Both numbers suggest that the cloud system consisted of relatively small ice crystals. In situ measurements frequently give larger crystals [e.g., *Auer and Veal,* 1970; *Dowling and Radke,* 1990]. In this respect we should bear in mind that ATSR-2 derived crystal sizes are representative for cloud top height (where crystals are most probably small because temperatures are low), whereas in situ measurements are usually made throughout the cloud.

Acknowledgment. Financial support for this research was provided by Space Research Organization Netherlands (SRON project EO-025).

References

Anderson, G. P., S. A. Clough, F. X. Kneizys, J. H. Chetwynd, and E. P. Shettle, AFGL atmospheric constituent profiles, Tech. Rep. *AFGL-TR-86-0110*, Air Force Geophys. Lab., Hanscom Air Force Base, Mass., 1986.

Auer, A. H., and D. L. Veal, The dimension of ice crystals in natural clouds, *J. Atmos. Sci., 27*, 919-926, 1970.

Baran, A. J., P. D. Watts, and J. S. Foot, Potential retrieval of dominating crystal habit and size using radiance data from a dual-view and multiwavelength instrument: A tropical cirrus anvil case, *J. Geophys. Res., 103*, 6075-6082, 1998.

Cai, Q., and K.-N. Liou, Polarized light scattering by hexagonal ice crystals: Theory, *Appl. Opt., 21*, 3569-3580, 1982.

Chepfer, H., G. Brogniez, and Y. Fouquart, Cirrus clouds' microphysical properties deduced from POLDER observations, *J. Quant. Spectrosc. Radiat. Transfer, 60*, 375-390, 1998.

De Haan, J. F., P. Bosma, and J. W. Hovenier, The adding method for multiple scattering calculations of polarized light, *Astron. Astrophys., 183*, 371-391, 1987.

De Rooij, W. A., and C. C. A. H. Van der Stap, Expansion of Mie scattering matrices in generalized spherical functions, *Astron. Astrophys., 131*, 237-248, 1984.

Dowling, D. R., and L. F. Radke, A summary of the physical properties of cirrus clouds, *J. Appl. Meteorol., 29*, 970-978, 1990.

Hess, M., and M. Wiegner, COP: A data library of optical properties of hexagonal ice crystals, *Appl. Opt., 33*, 7740-7746, 1994.

Hess, M., R. B. A. Koelemeijer, and P. Stammes, Scattering matrices of imperfect hexagonal ice crystals, *J. Quant. Spectrosc. Radiat. Transfer, 60*, 301-308, 1998.

Liou, K.-N., Influence of cirrus clouds on weather and climate processes: A global perspective, *Mon. Weather. Rev., 114*, 1,167-1,199, 1986.

Macke, A., *Modellierung der optischen Eigenschaften von Cirruswolken*, Ph. D. Thesis, 98 pp., Univ. of Hamburg, Germany, 1994.

Macke, A., J. Mueller, E. Raschke, Single scattering properties of atmospheric ice crystals, *J. Atmos. Sci, 53*, 2813-2825, 1996.

Nakajima, T., and M. D. King, Determination of the optical thickness and effective particle radius of clouds from reflected solar radiation measurements,. I, Theory, *J. Atmos. Sci., 47* (15), 1878-1893, 1990.

Potter, J. F., The delta function approximation in radiative transfer theory, *J. Atmos. Sci., 27*, 943-949, 1970.

Stammes, P., Errors in UV reflectivity and albedo calculations due to neglecting polarisation, Proc. SPIE Int. Soc. Opt. Eng., 2311, 227-235, 1994.

Stephens, G. L., S.-C. Tsay, P. W. Stackhouse, Jr., and P. J. Flatau, The relevance of the microphysical properties of cirrus clouds to climate and climatic feedback, *J. Atmos. Sci., 47* (14), 1742-1753, 1990.

Takano, and Y., K. Jayaweera, Scattering phase matrix for hexagonal ice crystals computed from ray optics, *Appl. Opt., 24*, 3254-3263, 1985.

Warren, S. G., Optical constants of ice from the ultraviolet to the microwave, *Appl. Opt., 23*, 1206-1225, 1984.

Watts, P. D., Potential use of Along Track Scanning Radiometer data for cloud parameter retrieval, *Proc. SPIE Int. Soc. Opt. Eng., 2578*, 30-45, 1995.

Watts, P. D., and A. J. Baran, A survey of tropical cirrus particle size and shape using ATSR-2 visible/near-infrared data, in

Proceedings of the 3rd ERS Symposium on Space at the Service of our Environment, Florence, Italy, 17-21 March, pp. 773-778, ESA Publications Division, ESTEC, Noordwijk, The Netherlands, 1997.

Watts, S. K., P. D. Watts, and A. J. Baran, Tropical cirrus cloud parameters from the Along Track Scanning Radiometer (ATSR-2), *Proc. SPIE Int. Soc. Opt. Eng.*, *3495*, 321-331, 1998.

Wendling, P., R. Wendling, H. K. Weickmann, Scattering of solar radiation by hexagonal ice crystals, *Appl. Opt.*, *18*, 2663-2671, 1979.

M. Hess, W. H. Knap, R. B. A. Koelemeijer, and P. Stammes, Royal Netherlands Meteorological Institute (KNMI), PO Box 201, 3730 AE De Bilt, The Netherlands. (hess@knmi.nl, knap@knmi.nl, koelemei@knmi.nl, stammes@knmi.nl)

P.D. Watts, Rutherford Appleton Laboratory (RAL), Chilton, Didcot, Oxon, OX11 0QX, United Kingdom. (watts@atsrpw.ag.rl.ac.uk).

(Received January 20, 1999; revised April 14, 1999;
accepted April 29, 1999.)